The Astrophysical Journal, 943:173 (6pp), 2023 February 1 https://doi.org/10.3847/1538-4357/acad75

A New Component from the Quiet Sun from Radio to Gamma Rays: Synchrotron Radiation by Galactic Cosmic-Ray Electrons

Elena Orlando[1,2], Vahe' Petrosian[2], and Andrew Strong[3]
[1] Department of Physics, University of Trieste, Italy; orlandele@gmail.com
[2] National Institute for Nuclear Physics (INFN) and Trieste Observatory of the Italian National Institute for Astrophysics (INAF), Italy
[3] Kavli Institute for Particle Astrophysics and Cosmology and Hansen Experimental Physics Laboratory, Stanford University, USA
Received 2022 September 30; revised 2022 December 18; accepted 2022 December 19; published 2023 February 7

Abstract

The quiet Sun, i.e., in its nonflaring state or nonflaring regions, emits thermal radiation from radio to ultraviolet. The quiet Sun also produces nonthermal radiation observed in gamma rays due to interactions of Galactic cosmic rays (GCRs) with the solar atmosphere and photons. We report on a new component: the synchrotron emission by GCR electrons in the solar magnetic field. To the best of our knowledge this is the first time this emission has been theoretically claimed and modeled. We find that the measured GCR electrons with energies from tens of GeV to a few TeV produce synchrotron emission in X-rays, which is a few orders of magnitude lower than current upper limits of the quiet Sun set by RHESSI and FOXSI, with no energy losses included. For a radially decreasing solar magnetic field we find the expected synchrotron intensity to be almost constant in the solar disk, to peak in the close proximity of the Sun, and to quickly drop away from the Sun. We also estimate the synchrotron emission from radio to gamma rays, and we compare it with current observations, especially with LOFAR. While it is negligible from radio to UV compared to the solar thermal radiation, this emission can potentially be observed at high energies with NuSTAR and more promising future FOXSI observations. This could potentially allow for constraining GCR densities and magnetic-field intensities at the Sun. This study provides a more complete description and a possible new way for understanding the quiet Sun and its environment.

Unified Astronomy Thesaurus concepts: Galactic cosmic rays (567); Cosmic rays (329); High-energy cosmic radiation (731); Quiet sun (1322); Solar radio emission (1522); Solar x-ray emission (1536)

1. Introduction

The quiet Sun, defined as its nonflaring state or nonflaring regions, is known to emit radiation from radio to gamma rays. While most of the radiation from the quiet Sun has thermal origin, at high energies it is produced by accelerated particles. In fact, the quiet gamma-ray emission above a few tens of MeV originates from interactions of Galactic Cosmic Rays (GCRs) with the solar atmosphere and the solar photons. In more detail, a disk component is supposed to be due to pion decay of GCR hadrons interacting with the solar atmosphere (Seckel et al. 1991; Thompson et al. 1997; Zhou et al. 2017; Niblaeus et al. 2019; Becker Tjus et al. 2020; Gutierrez & Masip 2020; Hudson et al. 2020; Li et al. 2020; Mazziotta et al. 2020), while a spatially extended component is supposed to be due to inverse Compton scattering of GCR electrons on the solar photon field (Moskalenko et al. 2006; Orlando & Strong 2007, 2021; Lai & Ng 2023). Both components were first observed with the Energetic Gamma Ray Experiment Telescope (Orlando & Strong 2008) and subsequently with the Fermi Large Area Telescope (Abdo et al. 2011; Barbiellini et al. 2014; Ng et al. 2016; Linden et al. 2018, 2020; Tang et al. 2018; Bartoli et al. 2019). In X-rays above a few keV (i.e., hard X-rays), the solar corona on its nonflaring state or nonflaring regions emits at millions of degrees, while the underlying chromosphere and photosphere are much cooler. This is known as the coronal heating problem, which is still one of the fundamental unanswered questions in solar physics (see, e.g., Caspi et al. 2015 and the review by Klimchuk 2006 and references therein). Nanoflares are among current possible explanations of the corona heating problem (Parker 1988). The Reuven Ramaty High Energy Solar Spectroscopic Imager (RHESSI; Lin et al. 2002), launched in 2003 and decommissioned in 2018, imaged the Sun and solar flares and provided spatially resolved spectroscopy with high spectral resolution from ∼3 keV to several MeV. RHESSI, the Focusing Optics X-Ray Solar Imager (FOXSI; Ishikawa 2014), and the Nuclear Spectroscopic Telescope Array (NuSTAR; Harrison et al. 2013) have recently provided solar observations above a few keV (Grefenstette et al. 2016), with RHESSI posing stringent upper limits to the quiet solar emission between 3 and 200 keV (Hannah et al. 2008, 2010) using almost 12 days of quiescent solar observations during solar minimum. These are still the deepest limits for solar hard X-ray emission yet reported for this energy range. At 3–6 keV and at 6–12 keV, these observations set upper limits at 3.4×10^{-2} photons s^{-1} cm^{-2} keV^{-1} and 9.6×10^{-4} photons s^{-1} cm^{-2} keV^{-1}, which have recently been confirmed by FOXSI (Buitrago-Casas et al. 2022) with just a few minutes of observations. Moreover, the FOXSI rocket mission assessed the hard X-ray flux of a quiescent solar region during a substantially high solar activity period for the first time. In the 5–10 keV energy range FOXSI-2 reached an upper limit of 4.5×10^{-2} photons s^{-1} cm^{-2} keV^{-1} during a period of high solar activity, and FOXSI-3 reached an upper limit of $9.3–6 \times 10^{-4}$ photons s^{-1} cm^{-2} keV^{-1} during a period of low solar activity. In the ∼1–15 keV energy range, the spectrophotometer Solar Photometer in X-rays (Sylwester et al. 2010) has measured the flux (counts s^{-1}) over inactive times from 2009 February 20 to 2009 October 10. In the radio band the quiet solar emission is

interpreted to be produced by thermal bremsstrahlung emission (e.g., Selhorst et al. 2005). In the optical band, in the UV band, and in the soft X-ray band (i.e., below a few keV) the solar emission is mostly of thermal origin. In the X-ray energy range, even during periods of low solar activity, the Sun's atmosphere is still filled with small-scale events like jets, flares, and minifilament eruptions. Here we introduce a new emission component of the quiet Sun from gamma rays to radio, with particular emphasis in the X-ray band, thanks to RHESSI and FOXSI upper limits. This nonthermal emission component is produced by synchrotron radiation of GCR electrons in the solar magnetic field. Section 2 explains our modeling and compares our estimates at high energies with the current data of the quiet Sun in X-rays by RHESSI and FOXSI. Section 3 discusses our predictions for future observations in X-rays, and it reports on our estimates of this synchrotron component from radio to UV in light of current and future observations.

2. Synchrotron Modeling and X-Ray Observations

In this section we report our calculations of the synchrotron emission by GCRs in the solar magnetic field, and we compare them with current observations.

The synchrotron emissivity is calculated numerically on a frequency grid and spatial grid in the heliosphere (x, y, ν) centered on the Sun. The spectrum and distribution of the synchrotron emissivity depend on the intensity of the magnetic field and the spectrum and distribution of GCR electrons at each point in the grid. For a randomly oriented magnetic field with intensity B and for an electron with Lorentz factor γ, the emissivity is isotropic and obtained with the formulation given by Ghisellini et al. (1988):

$$\epsilon(\nu, \gamma) = C\ q^2\Big[K_{4/3}K_{1/3} - \frac{3}{5}q(K_{4/3}K_{4/3} - K_{1/3}K_{1/3})\Big], \quad (1)$$

with $q = \nu/\nu_c; \nu_c = \frac{3}{2\pi}\frac{e}{mc}B\gamma^2; C = 2\sqrt{3}\frac{e^3}{mc^2}B$ erg s^{-1} Hz^{-1}; and $K_{4/3}$, $K_{1/3}$ Bessel functions, computed using the GNU Scientific Library.[4] From there, the relation between the characteristic synchrotron photon energy E, the GCR electron energy E_e, and the intensity of the magnetic field B follow the analytical approximation:

$$E \approx 67\ B\ (E_e/10^{12})^2, \quad (2)$$

with E in keV, E_e in eV, and B in G. To obtain the synchrotron intensity, we integrate the calculated emissivity over the line of sight. Hence, following Strong et al. (2011) and Orlando & Strong (2013) the synchrotron intensity along a line of sight s at frequency ν for a given isotropic distribution and spectrum of GCR electrons n_γ is given by

$$I(\nu) = \int\int \epsilon(\nu, \gamma)\, n_\gamma\, d\gamma\, ds. \quad (3)$$

As for the high-energy electrons involved in the synchrotron modeling in X-rays and gamma rays, which are produced by electrons above a few tens of GeV, we can consider the solar modulation of GCRs to be negligible (see, e.g., Li et al. 2022). For our synchrotron modeling we assume the GCR electron spectrum (electrons plus positrons) as measured by the Alpha Magnetic Spectrometer (AMS-02; Aguilar et al. 2014) and by the High Energy Stereoscopic System (HESS).[5] The assumed GCR electron spectrum is shown in Figure 1. The blue solid line shows the GCR electron spectrum that fits AMS-02 and HESS data. The plot also illustrates the AMS-02 (Aguilar et al. 2014), the Antimatter Matter Exploration and Light-nuclei Astrophysics (PAMELA; Adriani et al. 2011), the Dark Matter Particle Explorer (DAMPE; DAMPE Collaboration et al. 2017), and the HESS measurements. Below several hundreds of MeV, electrons are affected by solar modulation, which is why PAMELA and AMS-02 measurements differ. DAMPE measurements are somehow higher than AMS-02 in the region of interest for X-ray synchrotron emission, which makes our calculations conservative. However, here we neglect GCR energy losses, with the result that our estimates of the synchrotron intensity should be treated as an upper limit (see Section 3.3 for a deeper discussion) for the given magnetic-field models used.

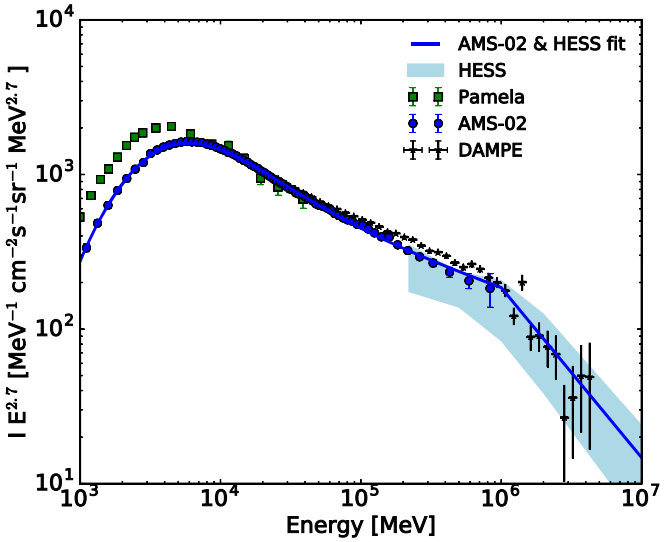

Figure 1. Modeled electron spectrum (solid blue line) compared with data. The model is fitted to the AMS-02 (Aguilar et al. 2014) electron spectrum for the period of 2013 (blue circles) and to HESS measurements (bluish region and black crosses). The bluish region identifies the HESS measurement's uncertainty. The electron spectrum measured by PAMELA (Adriani et al. 2011) is also shown (green squares), with measurements by DAMPE (black stars; DAMPE Collaboration et al. 2017). The plotted spectrum is used to calculate the synchrotron emission.

For calculating the synchrotron emission, we need to assume magnetic-field models. They are as in Petrosian et al. (2023) and described in the following. It is believed that the intensity of the magnetic field in the heliosphere follows a Parker spiral law with $B(r) \propto r^{-\delta}$ and $\delta \approx 2$ with r distance from the Sun, as confirmed by recent observations by Parker Solar Probe (Badman et al. 2021). We consider two regions for the magnetic field: the inner heliosphere from $0.1 < r/\mathrm{au} < 1$ and the region closer to the Sun with $r/\mathrm{au} < 0.1$. For the former, we assume the intensity of the magnetic field that fits recent observations by the Parker Solar Probe extending to about $20\,R_{\mathrm{Sun}}$ (or $r/\mathrm{au} = 0.1$). For the latter, we assume two different models as in the following: a model based on Gopalswamy & Yashiro (2011;

[4] http://www.gnu.org/software/gsl

[5] https://www.mpi-hd.mpg.de/hfm/HESS/pages/home/som/2017/09/

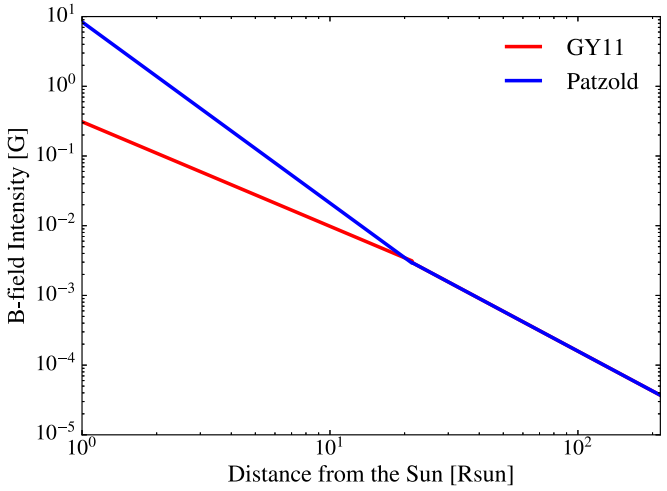

Figure 2. Assumed magnetic-field intensity as a function of the distance from the Sun in solar radii. Lines are analytical fits to the observed magnetic field as explained in the text and in Petrosian et al. (2023). The red line (GY11) shows the radial intensity based on Gopalswamy & Yashiro (2011) and Parker Solar Probe measurements (Badman et al. 2021). The blue line (Patzold) is based on the magnetic field as in Patzold et al. (1987) and Badman et al. (2021). For $r/\mathrm{au} > 0.1$ the GY11 and Patzold models assume a magnetic-field intensity based on the Parker Solar Probe measurements.

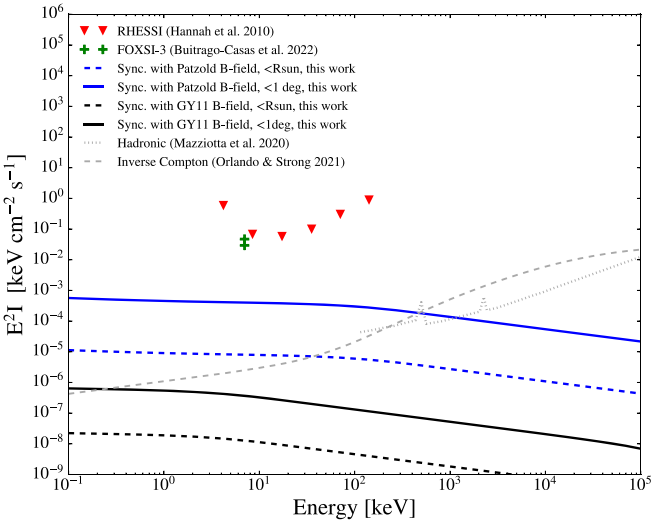

Figure 3. Calculated synchrotron spectral flux with the Patzold (blue lines) and GY11 (black lines) models. Dashed lines are obtained by integrating the emission in the entire solar disk; solid lines are obtained by integrating the emission in a disk of 1° from the center of the Sun. Red triangles are RHESSI flux upper limits for the entire solar disk. Green crosses are the FOXSI-3 upper limits of the quiet Sun. Also shown are the inverse Compton (Orlando & Strong 2021; gray dashed line) and the pion decay (Mazziotta et al. 2020; gray dotted line) model components.

we called it GY11), which derived the intensity variation in the region $5 < r/\mathrm{au} < 25$ by using observations of the corona mass ejections and a model based on Patzold et al. (1987; we called it Patzold), which agrees with Parker Solar Probe observations and steepens at the photosphere. Due to the current limited knowledge of the magnetic field at the Sun, we consider the two models above to bracket the uncertainty. Also, the different intensity between the two models accounts for possible different solar conditions. After assuming continuation in the point of transition between models, we obtain the following parameterization for the intensity of the magnetic field:

$$B(r) = \begin{cases} 1.0\,(r/R_{\rm sun})^{-1.9}, & \text{Parker Solar Probe for } 0.1 < r/\mathrm{au} < 1.0. \\ 0.31\,(r/R_{\rm sun})^{-1.5}, & \text{GY11, for } r/\mathrm{au} < 0.1. \\ 8.4\,(r/R_{\rm sun})^{-2.6}, & \text{Patzold, for } r/\mathrm{au} < 0.1 \end{cases}, \quad (4)$$

with $B(r)$ in Gauss. The intensity of the magnetic field as a function of the distance from the Sun in solar radii is reported in Figure 2.

Close to the Sun, in a magnetic field of a few G, synchrotron emission in the RHESSI energy band is produced mainly by electrons from a few tens of GeV to a few TeV (see, e.g., Equation (2)). We calculate the synchrotron emission up to 100 MeV where,[6] due to the relatively low magnetic-field strength, we can consider it to be in the classical regime.[7] Note that GCR electrons below several TeV are constrained by direct measurements. Because GCR electron direct measurements extend up to ∼10 TeV, which produce synchrotron emission up to a few tens of MeV for a magnetic field of several G, the electron spectrum is extrapolated up to 100 TeV. Figure 3 shows the calculated synchrotron spectral flux for the two magnetic-field models defined above: GY11 (black lines) and Patzold (blue lines). By comparing the two models, we see that the synchrotron flux is very sensitive to the magnetic-field intensity, which is not surprising because it scales as $B^{(p+1)/2}$, where $p \sim 3$ is the spectral index of the electrons. Models are compared with RHESSI (Hannah et al. 2010) and FOXSI (Buitrago-Casas et al. 2022) upper limits of the quiet Sun. The plotted observed upper limits were integrated for the entire solid angle of the Sun (I. Hannah 2020, private communication). We see that synchrotron emission produces X-rays in the energy band where upper limits to the quiet solar emission have been obtained. The expected synchrotron emission is a few orders of magnitude lower than current upper limits of the quiet Sun, which makes it promising to be observed in future. The same figure shows dashed lines that are obtained by integrating the emission in the entire solar disk and solid lines that are obtained by integrating the emission over a circular region of 1° radius from the center of the Sun. Note that the calculated synchrotron flux including the region outside the solar disk is larger than the calculated flux on the disk alone. To better investigate this effect and to understand which solar regions contribute the most to the entire flux, we show the calculated

[6] Synchrotron emission has a maximum energy photon around 200 MeV, above which radiation reaction becomes dominant and particles lose energy in a few orbits.

[7] Quantum mechanical effects become important when $(3/2) \times \gamma \times (B/B_{\rm cr}) > 1$, with $B_{\rm cr} = 4 \times 10^{12}$ G (see Brainerd & Petrosian 1987). For example, for $B = 10$ G, γ would need to be $>10^{11}$.

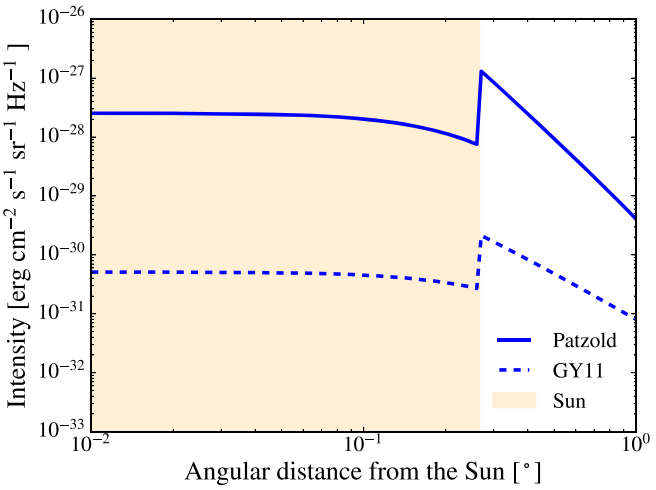

Figure 4. X-ray intensity profile of the synchrotron emission calculated at 10^{18} Hz with Patzold model (solid line) and with GY11 model (dashed line) of the magnetic field reported in Figure 2. The yellow region identifies the solar disk extension.

synchrotron intensity profile along the line of sight as a function of the angular distance from the center of the Sun (see Figure 4) for the two magnetic-field models. We find that, while the synchrotron intensity is almost constant in the solar disk, it significantly increases at the solar limb, and then, it quickly drops away from the Sun. This intensity profile is explained by a combination of two factors: the fact that GCR electrons do not penetrate inside the Sun and the fact that the magnetic field decreases with the distance from the Sun. The quick drop is explained by the following. Because the intensity of the magnetic field drops with the distance from the Sun, the synchrotron intensity quadratically depends on the magnetic-field intensity, as seen above. Hence, the radiation is more concentrated in the close proximity of the Sun. The results are that the magnetic field very close to the Sun mostly contributes to the synchrotron flux and that the synchrotron emission quickly drops away from the Sun. We find the integrated flux of synchrotron emission within the solar disk to be about 25% and 15% of the total flux from the Sun for the Patzold and GY11 models respectively, while the region outside $R_{\rm Sun}$ makes almost 75% and 85% of the total flux respectively.

3. Discussion

3.1. RHESSI Heredity and Predictions for NuSTAR and FOXSI

RHESSI (Hannah et al. 2010) has placed the lowest upper limits on the hard X-ray emission from the quiet Sun from 3 to 200 keV, allowing strong constraints on any energy released by nanoflares that fall below the RHESSI detection limit and even on axions possibly produced in the solar core. Improvements on the observed upper limits of the quiet Sun depend also on the sensitivity of the instrument to detect small flares. RHESSI has detected more than 25,000 transient X-ray microflares in the 6–12 keV energy band. Due to their spatial distribution from active regions, it is established that they do not heat the quiet corona (Christe et al. 2008; Hannah et al. 2008). NuSTAR observed the Sun several times since the start of solar pointing in 2014 September. The authors (Marsh et al. 2017) state that NuSTAR is sensitive to transient events several times smaller than the RHESSI detection threshold for identical integration times. During solar minimum they expect the NuSTAR sensitivity to increase by over 2 orders of magnitude due to higher instrument live time and reduced solar background. Its minimum detectable flux for 1 Ms of 1.7×10^{-6}, 2.9×10^{-6}, 1.0×10^{-4}, and 8.3×10^{-3} keV cm^{-2} s^{-1} at 3, 10, 30, and 78 keV, respectively (F. Harrison & K. Madsen 2022, private communication) is comparable to synchrotron intensities shown in Figure 3. However, even though the NuSTAR instrument has higher sensitivity than RHESSI, it also handles a limited amount of photons at a time (I. Hannah, private communication). As a result, many photons may come from the corona, hence, limiting observations. On the other hand, a FOXSI-type solar mission can both produce direct imaging like NuSTAR, and also it can handle the larger solar flux. FOXSI is the first solar-dedicated instrument to observe hard X-rays with focusing optics. FOXSI-4,[8] scheduled for 2024, will continue to improve upon direct solar imaging. A possible future FOXSI concept would allow enough observation time to further constrain the current hard X-ray quiet Sun limits. The quiet Sun may be observed in various solar activity conditions, and the synchrotron emission could be detected and studied in detail. The observed solar profile might be obtained and compared with our model expectations of the synchrotron emission. By observing the synchrotron solar profile, GCR density, and magnetic-field intensity, models could be tested, and their intensity at the Sun could be indirectly traced. Additionally, the synchrotron emission from GCRs needs also to be accounted for when searching for axions (Sikivie 1983), which are hypothesized dark matter particles from the Sun. Solar axions are hypothesized to be produced in the solar core via nuclear reactions and to be converted to X-rays in the presence of a strong magnetic field (e.g., Hudson et al. 2012). RHESSI has been used to search for faint X-ray emission from axions converting in coronal magnetic fields (e.g., Hannah et al. 2007).

3.2. Synchrotron Modeling and Observations from Radio to UV

In this section we calculate the synchrotron intensity by GCRs from radio to UV, and we compare it with observations. Recently, the Low-Frequency Array (LOFAR; Zhang et al. 2022) measured the solar brightness temperature ranging from $\sim 10^5$ to $\sim 10^6$ K in the 20–80 MHz range. As previously found, the size of the Sun measured by LOFAR increases with the decrease of the frequency, with a radius larger than the local plasma frequency radius. In fact, it is known that at very low frequencies (below ~0.1 GHz) the solar disk appears much bigger than its optical size, and its brightness gradually decreases and vanishes after several solar radii. For frequencies above several GHz, the size of the Sun appears similar to its visible counterpart. Hence, higher-frequency radio emission originates closer to the photosphere, while lower-frequency radio emission originates in the corona, which gives the Sun a larger dimension in the sky. In the following, we start by reporting and discussing our estimates of the synchrotron emission in radio, and by comparing it with current LOFAR observations, we test if synchrotron emission in the radio band can contribute to the larger radius seen at low frequencies. The GCR electrons producing synchrotron emission from a few MHz to 100 MHz have energies up to 100 MeV. Hence, we calculate the synchrotron emission by accounting for GCR

[8] https://foxsi.umn.edu/launches/foxsi-4

electron measurements at low energies from balloons (Beuermann et al. 1969; Hartman & Pellerin 1976) and from PAMELA (Adriani et al. 2011). The resulting synchrotron brightness temperature has an almost constant temperature in the disk and a higher temperature in the limb, and it drops with the angular distance from the Sun with a similar shape as found in X-rays. We find it to be 5–6 orders of magnitude lower with respect to the latest observations by LOFAR (Zhang et al. 2022); hence, it is not significant in the radio domain, so we do not plot it. Because the expected brightness temperature of the synchrotron emission is decreasing with the increase of the frequency, this emission from GCRs cannot be distinguished in the radio band, not even with current very low-frequency telescopes such as the forthcoming space mission the Sun Radio Interferometer Space Experiment (Lazio et al. 2022). Moreover, while at 1 MHz, the expected synchrotron brightness temperature in the proximity of the Sun reaches a few hundred kelvins for the Patzold model, at 10 MHz below or at the same level of the cosmic microwave background. For comparison the brightness temperature of the Galactic synchrotron background is $\sim 10^6$ K at 1 MHz (Orlando & Strong 2013). As a result, in the radio band, the synchrotron emission from the Sun can be considered negligible with respect to the other emission mechanisms. Recently, the Atacama Large Millimeter/submillimeter Array (ALMA), working in the frequency band 35–950 GHz, was also able to image the quiet Sun (Alissandrakis et al. 2022). However, it measured a brightness temperature around 6000 K, which is more than 11 orders of magnitude higher than what we find from the synchrotron emission by GCRs. At even lower wavelengths than ALMA, up to UV, the calculated expected synchrotron emission from the Sun is totally insignificant compared to the brightness temperature of the solar thermal radiation.

3.3. GCR Heliospheric Propagation and Energy Losses

Our current calculations of the synchrotron spectrum by GCRs can be considered as an upper limit to this emission, given the fact that we did not account for GCR energy losses. Here, we discuss the expected effect on our estimates if energy losses are considered. Energetic GCRs may lose energy by synchrotron and inverse Compton emission. A reduction of the intensity of the GCR electrons at the Sun would linearly reflect on a reduction of the intensity of the expected synchrotron emission. Uncertainties on the energy losses are very large and strongly depend on the choice of the transport parameters. Calculations of electron propagation in the heliosphere, including diffusion and energy losses, is beyond the present effort and reported elsewhere (Petrosian et al. 2023). Moreover, in additional further works we aim at eventually constraining energy loss parameters with improved detection of the quiet Sun in gamma rays originated by a different emission mechanism, such as the significantly observed inverse Compton emission (e.g., Orlando & Strong 2021). Based on these considerations and based on magnetic-field models that are built on present observations, we expect the solar synchrotron intensity from radio to gamma rays to be equal or lower than estimated here. Note that this does not change our conclusions.

4. Summary

Starting from current precise GCR electron measurements and recent solar and heliospheric magnetic-field observations, we have reported estimates of the synchrotron emission from gamma rays to radio in the direction of the Sun and in the heliosphere produced by GCR electrons in the solar magnetic field. To the best of our knowledge, this is the first time this emission component has been proposed and modeled. We have analyzed the expected synchrotron profile and found that it is almost constant within the solar disk, while it peaks in the very proximity of the Sun where the magnetic field is maximum, then rapidly falls away from the solar surface. By comparing our estimates with recent upper limits of the quiet solar emission by RHESSI in X-rays, we have found that the expected emission component is a few orders of magnitude lower than current upper limits. We have concluded that, even though it does not explain current RHESSI upper limits, this new emission component provides a more complete description of the quiet Sun and could be observed and studied in the near future. This could be promising for NuSTAR and especially for future FOXSI observations. We have also compared our calculation of the synchrotron brightness temperature from the Sun with latest observations of the quiet Sun in radio, especially with LOFAR, finding that the upper limits of the expected synchrotron emission component is of a few kelvins, i.e., 5–6 orders of magnitude lower than the brightness temperature currently measured in the 10–100 MHz range from the quiet Sun. We have also found that, from millimeters to UV, the synchrotron emission component is negligible compared to the brightness temperature of the solar thermal radiation. Hence, because the expected synchrotron emission is several orders of magnitude lower than what is observed from radio to UV, we have concluded that there is little prospect for its detection in this band. On the other hand, we have showed that this emission could, in the future, potentially be observed at high energies.

The authors thank I. Hannah, F. Harrison, J. Lazio, and K. Madsen for useful comments. E.O. acknowledges the ASI-INAF agreement No. 2017-14-H.0, the NASA grant No. 80NSSC20K1558. V.P. is supported by NASA Living With Star program grant NNH20ZDA001N-LWS.

ORCID iDs

Vahe' Petrosian https://orcid.org/0000-0002-2670-8942
Andrew Strong https://orcid.org/0000-0003-3799-5489

References

Abdo, A. A., Ackermann, M., Ajello, M., et al. 2011, ApJ, 734, 116
Adriani, O., Barbarino, G. C., Bazilevskaya, G. A., et al. 2011, PhRvL, 106, 201101
Aguilar, M., Aisa, D., Alvino, A., et al. 2014, PhRvL, 113, 121102
Alissandrakis, C. E., Bastian, T. S., & Nindos, A. 2022, A&A, 661, L4
Badman, S. T., Bale, S. D., Rouillard, A. P., et al. 2021, A&A, 650, A18
Barbiellini, G., Bastieri, D., Bechtol, K., et al. 2014, ApJ, 784, 118
Bartoli, B., Bernardini, P., Bi, X. J., et al. 2019, ApJ, 872, 143
Becker Tjus, J., Desiati, P., Döpper, N., et al. 2020, A&A, 633, A83
Beuermann, K. P., Rice, C. J., Stone, E. C., & Vogt, R. E. 1969, PhRvL, 22, 412
Brainerd, J. J., & Petrosian, V. 1987, ApJ, 320, 703
Buitrago-Casas, J. C., Glesener, L., Christe, S., et al. 2022, A&A, 665, A103
Caspi, A., Woods, T. N., & Warren, H. P. 2015, ApJL, 802, L2
Christe, S., Hannah, I. G., Krucker, S., McTiernan, J., & Lin, R. P. 2008, ApJ, 677, 1385

DAMPE Collaboration, Ambrosi, G., An, Q., et al. 2017, Natur, 552, 63
Ghisellini, G., Guilbert, P. W., & Svensson, R. 1988, ApJL, 334, L5
Gopalswamy, N., & Yashiro, S. 2011, ApJL, 736, L17
Grefenstette, B. W., Glesener, L., Krucker, S., et al. 2016, ApJ, 826, 20
Gutierrez, M., & Masip, M. 2020, APh, 119, 102440
Hannah, I. G., Christe, S., Krucker, S., et al. 2008, ApJ, 677, 704
Hannah, I. G., Hudson, H. S., Hurford, G. J., & Lin, R. P. 2010, ApJ, 724, 487
Hannah, I. G., Hurford, G. J., Hudson, H. S., Lin, R. P., & van Bibber, K. 2007, ApJL, 659, L77
Harrison, F. A., Craig, W. W., Christensen, F. E., et al. 2013, ApJ, 770, 103
Hartman, R. C., & Pellerin, C. J. 1976, ApJ, 204, 927
Hudson, H. S., Acton, L. W., DeLuca, E. E., et al. 2012, in ASP Conf. Ser. 455, 4th Hinode Science Meeting: Unsolved Problems and Recent Insights, ed. L. R. Bellot Rubio, F. Reale, & M. Carlsson (San Francisco, CA: ASP), 25
Hudson, H. S., MacKinnon, A., Szydlarski, M., & Carlsson, M. 2020, MNRAS, 491, 4852
Ishikawa, S.-n., Glesener, L., Christe, S., et al. 2014, PASJ, 66, S15
Klimchuk, J. A. 2006, SoPh, 234, 41
Lai, A., & Ng, K. 2023, arXiv:2211.15691
Lazio, T. J. W., Kasper, J. C., Romero-Wolf, A., Lux, J. P., & Neilsen, T. 2022, in United States National Committee of URSI National Radio Science Meeting (USNC-URSI NRSM) (Piscataway, NJ: IEEE), 340
Li, J.-T., Beacom, J. F., & Peter, A. H. G. 2022, ApJ, 937, 27
Li, Z., Ng, K. C. Y., Chen, S., et al. 2020, arXiv:2009.03888
Lin, R. P., Dennis, B. R., Hurford, G. J., et al. 2002, SoPh, 210, 3
Linden, T., Beacom, J. F., Peter, A. H. G., et al. 2020, PhRvD, 105, 063013
Linden, T., Zhou, B., Beacom, J. F., et al. 2018, PhRvL, 121, 131103
Marsh, A. J., Smith, D. M., Glesener, L., et al. 2017, ApJ, 849, 131
Mazziotta, M. N., Luque, P. D. L. T., Di Venere, L., et al. 2020, PhRvD, 101, 083011
Moskalenko, I. V., Porter, T. A., & Digel, S. W. 2006, ApJL, 652, L65
Ng, K. C. Y., Beacom, J. F., Peter, A. H. G., & Rott, C. 2016, PhRvD, 94, 023004
Niblaeus, C., Beniwal, A., & Edsjö, J. 2019, JCAP, 2019, 011
Orlando, E., & Strong, A. 2013, MNRAS, 436, 2127
Orlando, E., & Strong, A. 2021, JCAP, 2021, 004
Orlando, E., & Strong, A. W. 2007, Ap&SS, 309, 359
Orlando, E., & Strong, A. W. 2008, A&A, 480, 847
Parker, E. N. 1988, ApJ, 330, 474
Patzold, M., Bird, M. K., Volland, H., et al. 1987, SoPh, 109, 91
Petrosian, V., Orlando, E., & Strong, A. W. 2023, ApJ, in press
Seckel, D., Stanev, T., & Gaisser, T. K. 1991, ApJ, 382, 652
Selhorst, C. L., Silva, A. V. R., & Costa, J. E. R. 2005, A&A, 433, 365
Sikivie, P. 1983, PhRvL, 51, 1415
Strong, A. W., Orlando, E., & Jaffe, T. R. 2011, A&A, 534, A54
Sylwester, J., Kowalinski, M., Gburek, S., et al. 2010, EOSTr, 91, 73
Tang, Q.-W., Ng, K. C. Y., Linden, T., et al. 2018, PhRvD, 98, 063019
Thompson, D. J., Bertsch, D. L., Morris, D. J., & Mukherjee, R. 1997, JGR, 102, 14735
Zhou, B., Ng, K. C. Y., Beacom, J. F., et al. 2017, PhRvD, 96, 023015
Zhang, P., Zucca, P., Kozarev, K., et al. 2022, ApJ, 932, 17